Physica A 660 (2025) 130210

Contents lists available at ScienceDirect

Physica A

journal homepage: www.elsevier.com/locate/physa

Evolutionary dynamic of the coupled awareness-epidemic networks with higher-order structure

Xiangyu Meng [a], Wei Wei [a,d], Xiangnan Feng [b,*], Zhenyu Shi [c], Baifeng Li [d]

[a] Institute of Artificial Intelligence, Beihang University, Beijing, 100191, China
[b] Complexity Science Hub, Vienna, 1080, Austria
[c] Department of Automation, Shanghai Jiao Tong University, Shanghai, 200240, China
[d] School of Mathematical Sciences, Beihang University, Beijing, 100191, China

ARTICLE INFO

Keywords:
Multiplex network
Higher-order interactions
Mean-field approach
Evolutionary dynamics

ABSTRACT

Mitigating epidemic spreading and outbreaks is crucial to reducing their significant impacts on people's lives. Although research has begun to consider the impact of information networks on disease transmission in recent years, most studies have not fully considered the high-order characteristics in network structures. To better capture the dynamics of epidemic spreading and comprehensively understand and predict epidemic transmission patterns, a model of epidemic spreading in a coupled awareness-epidemic model, considering higher-order structures, is proposed. Extensive simulations on real and synthetic structured networks show that information networks influence the spread on physical contact networks by altering individual behaviors, leading to a transition from bistability to a single stable state induced by higher-order structures. Through theoretical analysis, it is proved that the corresponding conclusion is that as the information influence value (an indicator that measures the impact of information networks on physical contact networks) decreases, the impact of higher-order structures on the system's dynamic behavior gradually weakens. This leads to the disappearance of the bistable phenomenon originally caused by the presence of higher-order structures, and the system transitions from a bistable state to a single stable state. This transition is accompanied by an increase in the threshold for epidemic outbreaks and a decrease in the stable infection density. This work contributes to a deeper understanding of the influence of information on epidemic dynamics, providing important theoretical guidance for the future development of more effective prevention and control strategies.

1. Introduction

Complex networks comprehensively describe the interactions with various natural systems [1]. They are extensively used as the foundational – and possibly multilayered [2] – social structure for dynamic processes [3], including disease spreading [4], innovation diffusion and adoption [5], as well as opinion formation [6]. In the real world, the outbreak and spread of epidemics could severely disrupt daily life and make profound impacts on people's lives, such as the COVID-19 [7], the SARS virus [8], and influenza [9]. Consequently, the problem of effectively controlling disease transmission has attracted considerable attention [10].

The disease spreading not only conforms to the characteristics of simple disease transmission models but also can be influenced by various behaviors and interactions. These influences are often accompanied by other networks, such as information networks (online,

* Corresponding author.
E-mail addresses: weiw@buaa.edu.cn (W. Wei), feng@csh.ac.at (X. Feng).

https://doi.org/10.1016/j.physa.2024.130210
Received 30 August 2024; Received in revised form 22 October 2024
Available online 10 November 2024
0378-4371/© 2024 Elsevier B.V. All rights are reserved, including those for text and data mining, AI training, and similar technologies.

social networks) [11]. The diversified communication methods and the acceleration of information acquisition have profoundly impacted human society [12]. When facing global pandemics like COVID-19, timely access to information related to the epidemic becomes crucial since it aids in effectively addressing the challenges posed by the outbreak. Therefore, in recent years, an increasing number of scholars have begun to focus on the interaction between information dissemination dynamics and epidemic spreading to establish awareness-epidemic transmission models [13]. In these networks, one layer represents the physical contact network and the other represents the information network. Each layer has distinct connectivity patterns: disease transmission occurs within the physical network, while information exchange happens within the information network, with participants common to both [14]. The exchange of information leads to informed individuals taking a series of actions to curb the spread of disease within the physical contact network [15]. For example, some researchers have studied the impacts of different types of information dissemination on the epidemic spread, including the transmission modes of social media, news reports, and other channels [16]. Other studies have analyzed the influence of network topology on the interaction between perception diffusion and epidemic transmission, exploring the extent to which different network structures, such as scale-free networks and small-world networks [17]. In the disease transmission research, researchers usually consider the impact of epidemic-related information and more complex higher-order structural factors in addition to basic node and connectivity structures to enable more accurate prediction of disease spread dynamics [18].

Moreover, in the transmission process, contagion occurs in different ways: pairwise interactions (links in the network) or group interactions, which correspond to higher-order structures. Higher-order or group interactions, which arise from co-location activities, are common in offline/physical spatio-temporal interaction networks [19,20]. These interactions play an essential role in epidemic dynamics, as they increase the complexity of contact patterns. A person can be infected individually by every one of their neighbors (simple infection) or through continuous exposure to a group of neighbors (group exposure), as exemplified in real-life scenarios such as social gatherings [21] or aerosol transmission [22]. Investigating these group interactions aligns more closely with real-world conditions and the intricate dynamics of disease transmission. Additionally, residents in larger cities tend to have more frequent contacts, which can significantly influence epidemic spreading [23].

Previous studies have primarily focused on static network structures with pairwise interactions, such as the classical SIR and SEIR models [24], which have provided essential theoretical foundations for analyzing long-term disease transmission behavior and short-term outbreak characteristics. As research has progressed, scholars have gradually recognized the importance of information in disease transmission and began exploring the dynamics of coupled information and disease spread in complex networks. Funk et al. [25] proposed a mathematical model that establishes the relationship between epidemiology and disease-related information to analyze the spread of awareness within populations. Their study found that awareness related to epidemics can reduce disease incidence and even prevent its spread, especially when the disease is easily detected and information spreads rapidly. Subsequently, Granell et al. [26] developed a two-layer network model to represent the coupled spread of epidemics and disease-related information, discovering that information transmission can prevent outbreaks and trigger so-called subcritical spreading. They further introduced mass media into the model to examine its role in suppressing infectious disease outbreaks [27]. Guo et al. [28] proposed a threshold model to describe information transmission over multiplex networks, exploring the coupled spread of epidemic and awareness. Sun et al. [29] examined asymmetrical dynamics of epidemic propagation and awareness diffusion in multiplex networks, highlighting the importance of network topology and inter-layer dynamics. Similarly, Sun and Fu [30] explored competitive dual-strain SIS models with awareness programs in heterogeneous networks, analyzing how different network configurations influence epidemic outcomes. Their findings revealed that a node without awareness can only acquire information if the proportion of its aware neighbors exceeds a certain threshold.

However, these studies primarily focus on static network structures with pairwise interactions and their impact on epidemic thresholds. As research advances, scholars have discovered that disease transmission can exhibit more complex phenomena, such as bistability and limit cycles. For example, when high-order structures are considered, disease spread may exhibit bistable behavior [18], meaning that the system can switch between two different stable states depending on the initial conditions. Additionally, the emergence of limit cycles [31] indicates that disease transmission can display periodic outbreaks, a phenomenon frequently observed in real-world infectious diseases. To more comprehensively understand and predict the dynamics of disease spread in complex networks, this study proposes coupling information and disease networks with high-order structures. This approach aims to reveal the impact of high-order interactions on disease transmission dynamics, as well as the regulatory effect of information transmission on these dynamics, thereby providing new theoretical insights for developing more effective disease prevention strategies.

Therefore, this article aims to integrate information networks, physical contact networks, and their higher-order structures to systematically study and observe their impact on disease transmission dynamics and regulation mechanisms, providing theoretical support for more precise prevention strategies. We established a coupled awareness-epidemic model with high-order interactions. Based on the impact of information networks on the bistability of physical contact networks caused by high-order structures, we conducted numerical simulations on SocioPatterns collaboration and synthesis of structured networks, and analyzed the results. Besides, we analyzed this phenomenon from two aspects: the equilibrium point and stability of the system using by the mean-field method.

2. Model

In physical contact networks, considering the influence of high-order interactions may lead to bistability [18]. Under fixed transmission rates, diseases may converge to different states (disease-free or endemic) with different initial conditions. The dissemination of information can have a significant impact on the spread of diseases, which enables the intervention of information networks to pull the system back from an endemic state to a disease-free state, or prevent the transitioning from a disease-free state to an endemic state. Therefore, exploring how information networks affect the bistable phenomena in physical contact networks with high-order structures can better understand the spread of diseases.

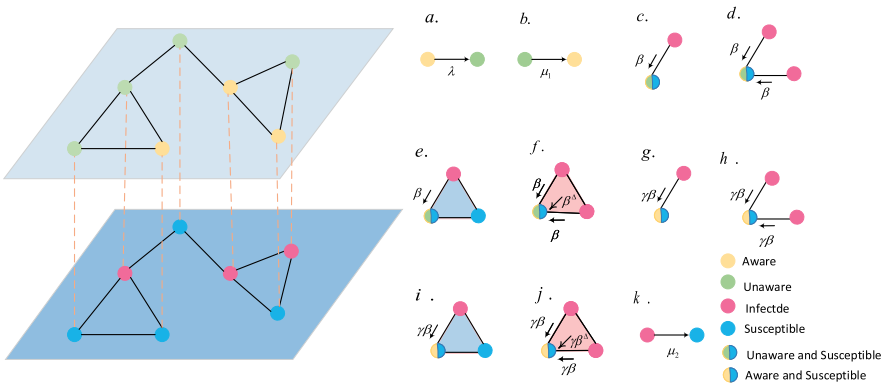

Fig. 1. A schematic diagram of the coupled awareness-epidemic network. The information network is based on the Unaware–Aware–Unaware (UAU) model, while the physical contact network is based on the Susceptible–Infectious–Susceptible (SIS) model, considering the influence of higher-order structures. In (a–b), the propagation process in the information network is depicted. Panels (c–f) depict the propagation process in the physical contact network with nodes that are unaware and susceptible, while (g–j) illustrate the process with nodes that are aware and susceptible. Specifically, (e) and (f) contrast scenarios with varying numbers of infectious nodes, illustrating the additional increase in infection probability through higher-order interactions when multiple infectious nodes are present. Panels (i) and (j) are similar in their depiction of these processes.

2.1. Coupled awareness-epidemic model with high-order interactions

We propose a awareness-epidemic model, where the physical contact network incorporates higher-order interactions, to characterize the interactions during epidemic transmission. Individuals will be in different states in both information diffusion and epidemic transmission. In the information network, information diffusion follows the Unaware–Aware–Unaware (UAU) model [32]: each node can be of either an aware (A) state or an unaware (U) state; an unaware node becomes aware with probability λ after communicating with an aware node; meanwhile, an aware node has a probability μ_2 forgetting epidemic-related information and thus transforms into an unaware state and stops transforming. In the physical contact network, the epidemic spread process is described by a Susceptible–Infectious–Susceptible (SIS) model [33] with higher-order structures. In this layer, a node can be in either an infectious (I) state or a susceptible (S) state. A susceptible node becomes infected with a probability β after contacting with an infected node. It can also be infected by the higher-order structures it is connected to, with an additional infection probability due to these higher-order interactions denoted as β^{Δ}. Similarly, an infected node recovers to the susceptible state with a probability μ_1.

It is important to note that the infection probability of susceptible individuals aware of the disease risk differs from those unaware. Susceptible individuals who recognize the disease risk exhibit a heightened sense of self-protection and are better prepared for the impending epidemic, which reduces their infection risk. To reflect this, the infection probability of a conscious susceptible individual upon contact is denoted as $\beta^A = \gamma\beta^U (\beta^U = \beta)$. This awareness also influences the infection effectiveness of higher-order structures on that node. The parameter γ represents the effectiveness of the self-protection measures taken by conscious susceptible individuals, ranging from 0 to 1. As γ approaches zero, self-protection measures become more effective; conversely, as γ approaches one, the efficacy of these measures diminishes. The parameter γ referred to as *information influence value* later in the paper.

2.2. Simplicial complexes

Typically, higher-order structures are characterized by hypergraphs or simplicial complexes. This study uses simplicial complexes to represent these higher-order structures, symbolizing the corresponding collective interactions. A simplicial complex is an aggregation of simplices and has varying dimensions [34]. A d-simplex, or simplex of dimension d, is a collection of $d+1$ nodes and describes $(d+1)$-body interactions. A 0-simplex is a node, a 1-simplex is a link, a 2-simplex (i, j, k) is a two-dimensional object made by three nodes, i.e. a (full) triangle, a 3-simplex is a tetrahedron, and so on.

A simplicial complex $\mathcal{S}$ defined on a given set of nodes $\mathcal{V}$, where $|\mathcal{V}| = N$, comprises a set of M-simplexes $\mathcal{S} = \{\rho_1, \rho_2, \ldots, \rho_M\}$. This means that all the simplexes built from subsets of ρ are also contained in $\mathcal{S}$. We indicate the number of d-simplexes in $\mathcal{S}$ as M_d, where $d = 1, 2, \ldots, D$ (where D is the dimension of the largest simplex in $\mathcal{S}$), with the constraint $\sum_{d=1}^{D} M_d = M$.

We use the adjacency matrix to present simplicial complexes mathematically. The adjacency matrix A of a graph $\mathcal{G}(\mathcal{V}, \xi)$ ($\mathcal{V}$ represents the set of nodes on the graph, ξ represents the set of edges on the graph) is an $N \times N$ matrix with entry $a_{ij} = 1$ when the edge $(i, j) \in \xi$, and 0 otherwise. In the case of simplicial complexes, consider tensors instead of matrices. In fact, for each dimension d, we can define the $\underbrace{N \times N \times \cdots \times N}_{d+1}$ adjacency tensor $A^{(d)}$, whose entry $a^{(d)}_{i_1,\ldots,i_{d+1}}$ is equal to 1 if the d-simplex $(i_1, \ldots, i_{d+1})$ belongs to the simplicial complex $\mathcal{S}$, and 0 otherwise. Notice that each tensor is symmetric with respect to its $d+1$ indices, namely the value of a given entry $a^{(d)}_{i_1,\ldots,i_{n+1}}$ is equal to the value of the entries corresponding to any permutation of its indices. According to the above definition, $A^{(1)}$ coincides with the standard adjacency matrix A, while the $N \times N \times N$ adjacency tensor [35] $A^{(2)}$

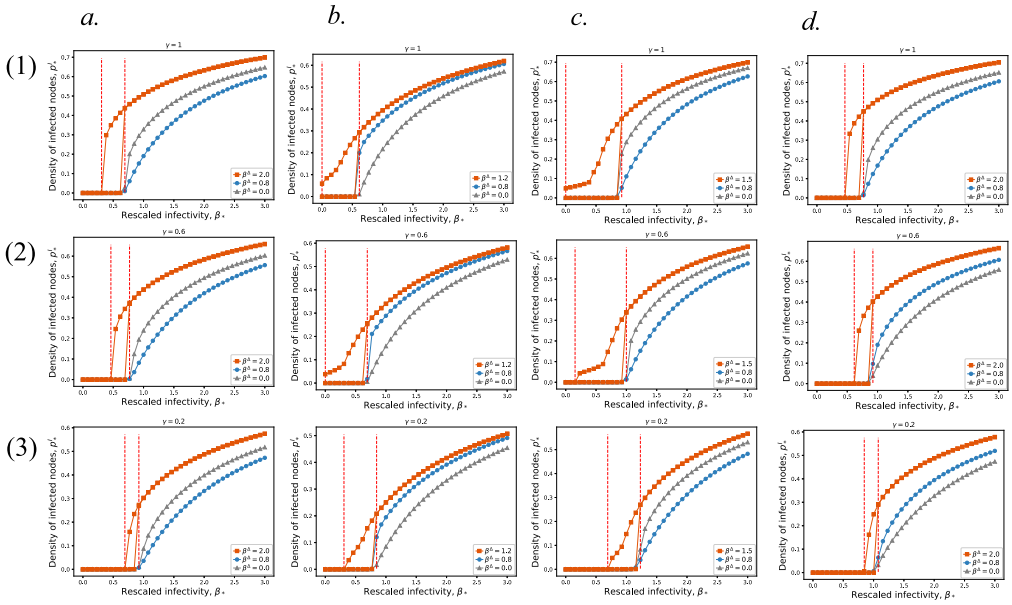

Fig. 2. Consideration of high-order structures on coupled awareness-epidemic model simulations in the SocioPatterns collaboration. Derived from detailed face-to-face contact records in four environments: a. workplace, b. conference, c. high school, and d. high school. High-order structures are considered as simplicial complex with $D = 2$, when the information influence value $\gamma = 1$, meaning there is no influence from the information network on the physical contact network, the prevalence curves are shown in panels a(1), b(1), c(1), and d(1). In this case, the coexistence of healthy and epidemic states is observed. When $\gamma = 0.6$, indicating that the information network begins to influence the physical contact network, the prevalence curves are shown in panels a(2), b(2), c(2), and d(2). As the influence further increases with $\gamma = 0.2$, the prevalence curves are displayed in panels a(3), b(3), c(3), and d(3). Here, the relationship between the mean proportion of infected nodes derived from numerical simulations and the rescaled infectivity $\beta_* = \frac{\beta\langle k_1\rangle}{\mu_1}$ is plotted. This is done for different rescaling parameters $\beta_*^A = \frac{\beta^A\langle k_1^A\rangle}{\mu_1}$, namely $\beta_*^A = 0.8$ (blue circles) and $\beta_*^A = 1.5$ (orange squares). The gray circles represent simulation curves of the equivalent conventional SIS model ($\beta_*^A = 0$), which indicates that higher-order interactions do not contribute any additional infection risk in the physical contact network. The horizontal axis represents rescaled infectivity β_*. The vertical axis represents density of infected nodes p_*^I.

characterizes two-dimensional objects: one has $a_{ijk}^{(2)} = 1$ if the three nodes i, j, k form a full triangle, and otherwise $a_{ijk}^{(2)} = 0$. In this way, it is possible to map completely the connectivity structure of a simplicial complex S into the entire set of D adjacency tensors $A^{(d)}$, where $d = 1, 2, \ldots, D$. We focus on simplicial complexes of dimension up to $d = 2$ in this article.

3. Result

3.1. Simulation in the SocioPatterns collaboration

Firstly, to explore the disease spread in coupled awareness-epidemic network with high order interactions, consider their evolution in empirical social structures. For this purpose, we refer to publicly available datasets depicting face-to-face interactions gathered by the SocioPatterns collaboration [36]. These are typical examples of group meetings that can be naturally encoded as simplices, differing in a set of binary interactions. We analyze interaction data gathered in four distinct social settings: a workplace ($InVS15$) [37], a conference ($SFHH$) [38], a middle school($LyonSchool$) [39] and a high school ($Thiers13$) [40]. For each scenario, the face-to-face interactions were recorded at a time resolution of 20 s. Next, we applied appropriate augmentation techniques [41] (detailed in Appendix A) to the data to observe bistability phenomena better. Table 1 presents the average generality of the four real-world simplicial complexes in the dataset both before and after undergoing data augmentation [42]. These augmented simplicial complexes are simulated as the physical contact network depicted in Fig. 2. To better simulate the impact of information network on physical contact network and eliminate bias, we construct an information network by randomly adding and removing edges on the physical contact network while keeping the average degree of its nodes.

3.1.1. Simulation process

The simulations are conducted on coupled awareness-epidemic model built from four datasets. We use the Microscopic Markov Chain Approach (MMCA) [43] for the corresponding simulation, with the relevant method detailed in Appendix B. Specifically, each simulation begins with an initial infection node density of $p^I(0)$ and proceeds with the transmission processes in the information network as shown in Fig. 1(a–b) [26] and all possible infection pathways in the physical contact network as depicted in Fig. 1(c–k). The information network has a corresponding influence on the physical contact network. If a state of absorption is attained (i.e., where there are no susceptible individuals), the simulation is halted. Otherwise, the average steady-state density of infected

Table 1
Statistics of real-world networks.

Dataset	Context	$\langle k \rangle$	$\langle k^{\Delta} \rangle$	$\langle k \rangle^{aug}$	$\langle k^{\Delta} \rangle^{aug}$
InVS15	Workplace	16.9	6.9	24.5	6.9
SFHH	Conference	15.0	7.6	20.5	10.8
LyonSchool	Middle school	19.4	4.1	22.2	4.2
Thiers13	High school	20.1	10.6	32.0	10.8

$\langle k \rangle$ denotes the average degree of nodes, $\langle k^{\Delta} \rangle$ denotes the average number of 2-simplices, $\langle k \rangle^{aug}$ denotes the average degree of nodes after undergoing data augmentation, $\langle k^{\Delta} \rangle^{aug}$ denotes the average number of 2-simplices after undergoing data augmentation.

Table 2
Description of symbols.

Symbol	Description
U	Unaware state in the information network
A	Aware state in the information network
S	Susceptible state in the physical contact network
I	Infectious state in the physical contact network
λ	The information transmission rate
β	The infection rate if in Unaware state
β^{A}	The infection rate if in Aware state
μ_1	The information forgetting rate
μ_2	The recovery rate
γ	Effectiveness of self-protection measures (information influence value)
N	Number of nodes in the network
p_1	Probability of generating links
p_2	Probability of generating 2-simplices
D	Dimensionality constraint of the simplicial complex
$\langle k_1 \rangle$	Average degree of nodes in the physical contact network
$\langle k_1^{\Delta} \rangle$	The average number of 2-simplices in the physical contact network
$\langle k_2 \rangle$	Average degree of nodes in the information network

nodes p_*^I is calculated by averaging the values measured during the last 100 steps once a stable condition is reached. These outcomes are based on the average of 50 runs, where the initial infection nodes are randomly distributed with a consistent density denoted as $p^I(0)$.

Furthermore, different datasets correspond to different densities of one-dimensional and two-dimensional simplicial complexes (refer to Table 1). Due to variations in the mean degrees and the mean numbers of two-dimensional simplicial complexes across different datasets, we adjust the transmission probabilities to observe phenomena near the thresholds better. The infectiousness parameters β and β^{Δ} are rescaled according to the average degree $\langle k_1 \rangle$ of the nodes and the average number of two-dimensional simplicial complexes $\langle k_1^{\Delta} \rangle$ occurring on the nodes, respectively. Simultaneously, different information influence values γ are adopted to represent the influence of the information network on the physical contact network. All results are presented by rescaled parameters $\beta_* = \frac{\beta \langle k_1 \rangle}{\mu_1}$ and $\beta_*^{\Delta} = \frac{\beta^{\Delta} \langle k_1^{\Delta} \rangle}{\mu_1}$, which allows for a more nuanced understanding of the interplay between the information and physical contact network. The corresponding symbol descriptions can be found in Table 2.

3.1.2. Simulation results

Fig. 2 displays the epidemic prevalence curves for four datasets. In each panel (Fig. 2a(1), b(1), c(1), d(1)), considering the information influence value γ as 1, representing the scenario where the information network does not influence the physical contact network, the graph illustrates the relationship between the average proportion of infected nodes at the steady state p^I and the rescaled transmissibility β_* in the simple contagion model. Here, $\beta_*^{\Delta} = 0.8$ (blue circles) and $\beta_*^{\Delta} > 1$ (orange squares) are depicted. For comparison, the case of $\beta_*^{\Delta} = 0$ is also illustrated, corresponding to the conventional SIS model without considering higher-order influences (gray triangles), revealing the presence of bistability regions influenced by higher-order structures under different initial conditions.

In each panel (Fig. 2a(2), b(2), c(2), d(2)), where the information influence value γ is set to 0.6. This configuration represents a scenario where the information network inhibits the physical contact network. Under these conditions, we observe that the range of bistability regions diminishes, and the entire bistability region shifts leftward. These phenomena indicate the reduction in the threshold for disease outbreaks. Similarly, by further reducing the information influence value to 0.2, in each panel (Fig. 2a(3), b(3), c(3), d(3)), it was found that the bistable region further narrowed and continued to move to the left. These observations underscore the significant impact of the information network on the bistability phenomena induced by higher-order structures within the physical contact network.

On different datasets, we observed the following phenomenon: in the $InVS15$ and $Thiers13$ datasets, as the influence of information increases, the bistable region of high-order structures gradually decreases and hysteresis [44] effects appear. In the $SFHH$ and $LyoSchool$ datasets, due to their topological characteristics, even if the disease infectivity is low, a certain infection density can still be maintained in the population when the information impact is not significant. However, as the influence of

information increases, the bistable interval gradually lags behind and shrinks.

Further explanation of the aforementioned phenomenon: In the context of the physical contact network, high-order structure refers to nonlinear effects caused by the interaction patterns within the network, which may include complex interactions along transmission paths or tight connections among groups. When an information network intervenes, it has the potential to modify the initial structure of the transmission network by impacting individual behaviors or the dissemination of information.

In the observed scenarios above, distinct behaviors are noted for two nonzero β^{Δ} values when disregarding the influence of information network layer on physical contact network, i.e., when the information influence value γ equals 1. For $\beta_*^{\Delta} = 0.8$, the change in the density of infected nodes with respect to β_* mirrors that of $\beta_*^{\Delta} = 0$ (simple contagion), displaying a continuous transition. For $\beta_*^{\Delta} > 1$, localized epidemic states with $p^I > 0$ appear at the epidemic threshold β_*^c, which is noticeably lower than the other two cases. Moreover, this transition is discontinuous, exhibiting hysteresis loops in the bistability region, where both healthy $p_*^I = 0$ and localized epidemic $p_*^I > 0$ states can coexist (as indicated by the dashed orange line). Notably, the final state in this parameter region depends on the initial density of infected nodes $p^I(0)$. When considering the influence of information network on physical contact network, i.e., $0 < \gamma < 1$, although γ continuously approaches 0, this discontinuous transition generated by higher-order structures gradually becomes continuous, and the bistable region continuously shrinks or even disappears.

3.2. Simulation in synthetic structured networks

The simplicial complexes in these simulations correspond to one-simplices and two-simplices with different social contexts and densities, yielding similar phenomenology. However, the generalized degree distributions exhibited by these empirical structures are not highly concentrated around their mean values, making it difficult to systematically explore size effects. To gain a deeper understanding of the phenomena within the simplicial contagion model, we turn our focus to investigating its behavior on synthetic simplicial complexes with controlled attributes.

3.2.1. Construction of a synthetic structured network

We use the Random Simplicial Complex model [18] to generate simplex simplicial models of different dimensions, which allows for maintaining a fixed average degree $\langle k_1 \rangle$ of nodes while varying the expected number $\langle k_1^{\Delta} \rangle$ of "full" triangles (2-simplices) on nodes. In this study, the model is constrained to $D = 2$, which confines the necessary parameters to (N, p_1, p_2) where N represents the number of nodes, and p_1 and p_2 represent the probabilities of generating links and generating 2-simplices, respectively. Further, this process can be easily extended to larger D. For any given size N, simplicial complexes with desired $\langle k_1 \rangle$ and $\langle k_1^{\Delta} \rangle$ values can be generated by appropriately adjusting p_1 and p_2, to constitute physical contact network. Similarly, when constructing information network by randomly adding and removing edges to the physical contact network, This approach reflects the fact that information spreads through different channels and social structures than physical contact network.

Simulations were performed using the described process on the coupled awareness-epidemic model created, with $N = 2000$ nodes, $p_1 \approx 0.04$, $p_2 \approx 3\times10^{-6}$, $\langle k_1 \rangle$ around 20, and $\langle k_1^{\Delta} \rangle$ around 6. For the information network layer, the network is constructed by removing 20% of the nodes from the physical contact network and adding 20% more nodes to form new links. Similar to real-world coupled awareness-epidemic model, $p^I(0)$ percent of seed infectious nodes were randomly placed in the physical contact network, while fixed seed infectious nodes were randomly placed in the information network. The average steady-state density of infection p_*^I was calculated by averaging overruns with different instances of the model for different information influence values γ.

3.2.2. Simulation results

In Fig. 3, we observe that the network of synthetic structures exhibits bistability regions when $\gamma = 1$ and $\gamma = 0.8$, indicating the presence of two stable states in the system: one representing a healthy state and the other indicating a disease outbreak state. However, as γ decreases to 0.2 and 0, we observe the disappearance of these bistability regions and an increase in the threshold for disease outbreak. This suggests that as the influence of the information network increases, characterized by the decrease in γ, the system's stability undergoes significant changes. The previously unstable states induced by high-order structures in the system gradually converge towards stable states, while the conditions required for disease outbreaks become more stringent.

In synthetic simplicial complex composite with controllable attributes, we observe a phenomenon that as information network influence γ decreases, the bistability regions gradually diminish and eventually disappear. This implies that increased information propagation weakens the system's bistability, leading it to tend more towards a single stable state.

Therefore, through the intervention of information dissemination, an information network can influence the high-order structure within the physical contact network, thereby altering the range and characteristics of bistability phenomena. Specifically, as the information influence value γ of the information network decreases, the increase in the influence of the information network may strengthen its regulation over individual behaviors within the physical contact network, thus suppressing the influence of high-order structures in the original network. This may lead to the bistability region's reduction or complete disappearance, as the physical contact network is no longer influenced by high-order structures and exhibits a single stable state.

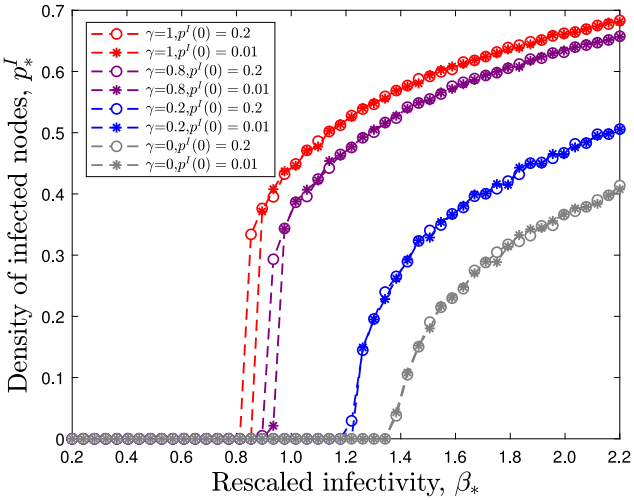

Fig. 3. The simulation results of the coupled awareness-epidemic model, where the physical contact network is constituted by synthetic simplicial complexes with controlled attributes, with $\gamma = 1$ (*red*), $\gamma = 0.8$ (*purple*), $\gamma = 0.2$ (*blue*), and $\gamma = 0$ (*gray*), $\circ$ representing $p^I(0) = 0.01$, and $*$ representing $p^I(0) = 0.2$. The horizontal axis represents rescaled infectivity β_*. The vertical axis represents density of infected nodes p_*^I.

3.3. Mean field approach

The mathematical expression of the above propagation process is particularly significant in determining how the disease evolves over time. In this study, we employ the mean-field method [45] to derive the state evolution equation of each state.

We model the evolution of the densities of the four states in the network on the corresponding propagation processes. The evolution process is illustrated in Fig. 4.

$$\begin{aligned}
\frac{dp^{SU}}{dt} =& \mu_1 p^{IU} + \mu_2 p^{SA} - p^{SU}\beta\langle k_1\rangle(p^{IA}+p^{IU}) - p^{SU}\beta^{\Delta}\left\langle k_1^{\Delta}\right\rangle \\
& (p^{IA}+p^{IU})^2 - p^{SU}\lambda\langle k_2\rangle(p^{IA}+p^{SA}), \\
\frac{dp^{IU}}{dt} =& -\mu_1 p^{IU} + \mu_2 p^{IA} + p^{SU}\beta\langle k_1\rangle(p^{IA}+p^{IU}) + p^{SU}\beta^{\Delta}\left\langle k_1^{\Delta}\right\rangle \\
& (p^{IA}+p^{IU})^2 - p^{IU}\lambda\langle k_2\rangle(p^{IA}+p^{SA}), \\
\frac{dp^{SA}}{dt} =& -\mu_2 p^{SA} + \mu_1 p^{IA} + p^{SU}\lambda\langle k_2\rangle(p^{IA}+p^{SA}) - p^{SA}\gamma\beta\langle k_1\rangle \\
& (p^{IU}+p^{IA}) - p^{SA}\gamma\beta^{\Delta}\left\langle k_1^{\Delta}\right\rangle(p^{IU}+p^{IA})^2, \\
\frac{dp^{IA}}{dt} =& -\mu_2 p^{IA} - \mu_1 p^{IA} + p^{IU}\lambda\langle k_2\rangle(p^{IA}+p^{SA}) + p^{SA}\gamma\beta\langle k_1\rangle \\
& (p^{IU}+p^{IA}) + p^{SA}\gamma\beta^{\Delta}\left\langle k_1^{\Delta}\right\rangle(p^{IU}+p^{IA})^2.
\end{aligned} \tag{1}$$

After introducing these two variables $p^I = p^{IU}+p^{IA}$ and $p^A = p^{SA}+p^{IA}$ with the additional condition that $p^{SU}+p^{IU}+p^{SA}+p^{IA} = 1$, we ultimately obtained a coupled system of equations:

$$\begin{aligned}
\frac{dp^I}{dt} =& -\mu_1 p^I + (\beta\langle k_1\rangle p^I + \beta^{\Delta}\left\langle k_1^{\Delta}\right\rangle(p^I)^2)[1 - p^I + (p^{IA} - p^A)(1-\gamma)], \\
\frac{dp^A}{dt} =& -\mu_2 p^A + (1-p^A)\lambda\langle k_2\rangle p^A, \\
\frac{dp^{IA}}{dt} =& -(\mu_1+\mu_2)p^{IA} + (p^I - p^{IA})\lambda\langle k_2\rangle p^A + (p^A - p^{IA})\gamma(\beta\langle k_1\rangle p^I + \beta^{\Delta}\left\langle k_1^{\Delta}\right\rangle(p^I)^2).
\end{aligned} \tag{2}$$

This differential equation System (1) has four variables. Through gradual simplification, a differential equation System (2) containing three variables p^I, p^A, and p^{IA} is obtained. Here, p^I represents the ratio of individuals in state I, and p^A in state A.

Next, we analyze the infection equilibrium point of the above equations to evaluate the impact of information network by higher-order structures. The equilibrium point of disease transmission refers to the state in which the disease transmission rate within a group reaches equilibrium, namely the average number of new infections transmitted by each infected individual remains unchanged. Analyzing the equilibrium point of disease transmission can help understand the situation and characteristics of disease transmission within the population, thus developing effective prevention and control measures.

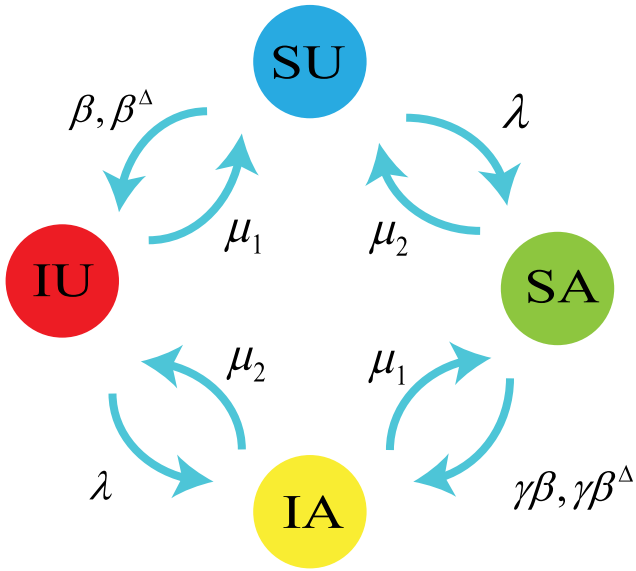

Fig. 4. Schematic diagram of the evolution process of four states in the network. β represents the disease infection rate, β^{Δ} represents the disease high-order action infection rate, λ represents the information network infection rate, μ_1 and μ_2 represent the disease network and information network recovery rate, respectively, and γ represents the information influence value.

An infection equilibrium $E_* = (p_*^I, p_*^A, p_*^{IA})$ is derived by setting the right part of system (2) equal to 0:

$$\begin{aligned}
&-\mu_1 p^I + (\beta\langle k_1\rangle p^I + \beta^{\Delta}\langle k_1^{\Delta}\rangle (p^I)^2)[1 - p^I + (p^{IA} - p^A)(1-\gamma)] = 0,\\
&-\mu_2 p^A + (1-p^A)\lambda\langle k_2\rangle p^A = 0,\\
&-(\mu_1+\mu_2)p^{IA} + (p^I - p^{IA})\lambda\langle k_2\rangle p^A + (p^A - p^{IA})\gamma(\beta\langle k_1\rangle p^I + \beta^{\Delta}\langle k_1^{\Delta}\rangle (p^I)^2) = 0.
\end{aligned} \tag{3}$$

It means $p_*^A = 1 - \frac{\mu_2}{\lambda\langle k_2\rangle}$, and we obtain

$$p_*^{IA} = \frac{\mu_1}{\beta\langle k_1\rangle + \beta^{\Delta}\langle k_1^{\Delta}\rangle p^I(1-\gamma)} - \frac{1-p^I}{1-\gamma} + p_*^A. \tag{4}$$

Then we can get p_*^I by solving $f(p_*^I) = 0$, with:

$$f(p_*^I) = A(p_*^I)^4 + B(p_*^I)^3 + C(p_*^I)^2 + Dp_*^I + E, \tag{5}$$

where the parameters A, B, C, D, and E are as follows:

$$\begin{aligned}
A =& -\gamma(\beta^{\Delta})^2\langle k_2^{\Delta}\rangle\lambda\langle k_2\rangle,\\
B =& \gamma\langle k_1^{\Delta}\rangle\beta^{\Delta}(\langle k_1^{\Delta}\rangle\beta^{\Delta} - 2\beta\langle k_1\rangle)\lambda\langle k_2\rangle,\\
C =& -\langle k_2\rangle\lambda(((\lambda\langle k_2\rangle - 2\beta\langle k_1\rangle - \mu_2 + \mu_1)\gamma + \mu_2 + \mu_1)\langle k_1^{\Delta}\rangle\beta^{\Delta} + \gamma\beta^2\langle k_1^2\rangle),\\
D =& -\gamma\lambda^2(\beta\langle k_1\rangle - \langle k_1^{\Delta}\rangle\beta^{\Delta})\langle k_2^2\rangle + \lambda((-\langle k_1^{\Delta}\rangle(\mu_2-\mu_1)\beta^{\Delta} + \beta\langle k_1\rangle(\beta\langle k_1\rangle + \mu_2 - \mu_1))\gamma\\
&+ \beta^{\Delta}\mu_2\langle k_1^{\Delta}\rangle - \beta\langle k_1\rangle(\mu_1+\mu_2))\langle k_2\rangle - \mu_2\mu_1\langle k_1^{\Delta}\rangle\beta_{\Delta}(\gamma-1),\\
E =& (\lambda(\gamma\beta\langle k_1\rangle - \mu_1)\langle k_2\rangle - \beta\langle k_1\rangle\mu_2(\gamma-1))(\lambda\langle k_2\rangle + \mu_1).
\end{aligned} \tag{6}$$

The corresponding solutions can be obtained by solving a univariate quartic equation, which relates to the values of disease density after the disease spread has reached a corresponding steady state. We substitute the solutions of the System (5) into the System (4) to obtain the equilibrium points and calculate the Jacobian determinant corresponding to the equilibrium points to determine their stability.

3.3.1. Analysis of equilibrium points and stability

Under different degrees of information impact denoted by γ, the conditions for the existence of equilibrium points lead to different outcomes. Fig. 5(a) illustrates the equilibrium points obtained by solving System (2) under different γ. As shown in Fig. 5(a), when $\gamma = 1$, bistability phenomena occur in the presence of higher-order structures. In this case, two different thresholds are derived: $\beta_{*1}^0 \approx 0.846$ and $\beta_{*1}^c = 1$, resulting in bistability phenomena. When $\gamma = 0.2$, the bistability phenomena disappear, leaving only one threshold $\beta_{*2}^c \approx 1.326$.

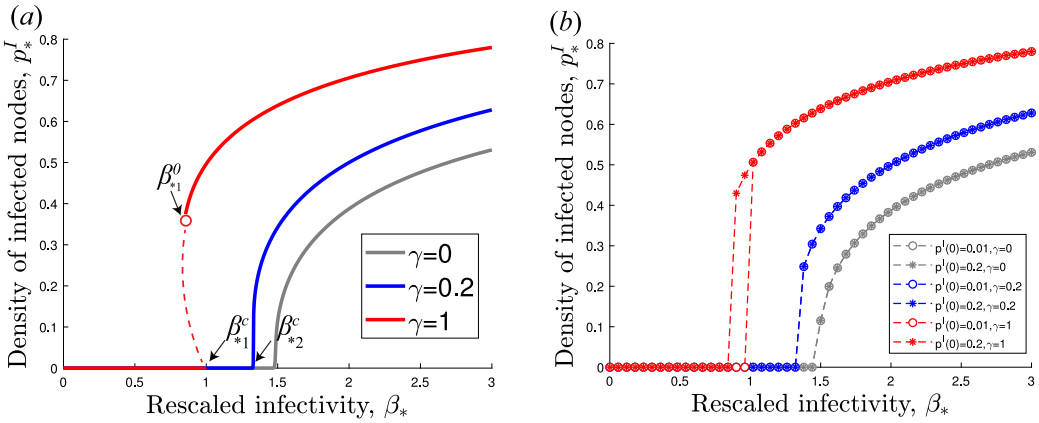

Fig. 5. (a) The system's equilibrium points under different information values impact factor γ. (b) Numerical solutions of the system at $t = 500$ under different values of information impact factor γ and initial infection density $p^I(0) = 0.01$ or 0.2. For both cases, set $\mu_1 = \mu_2 = 0.05$. The horizontal axis represents rescaled infectivity β_*. The vertical axis represents the density of infected nodes p^I_*.

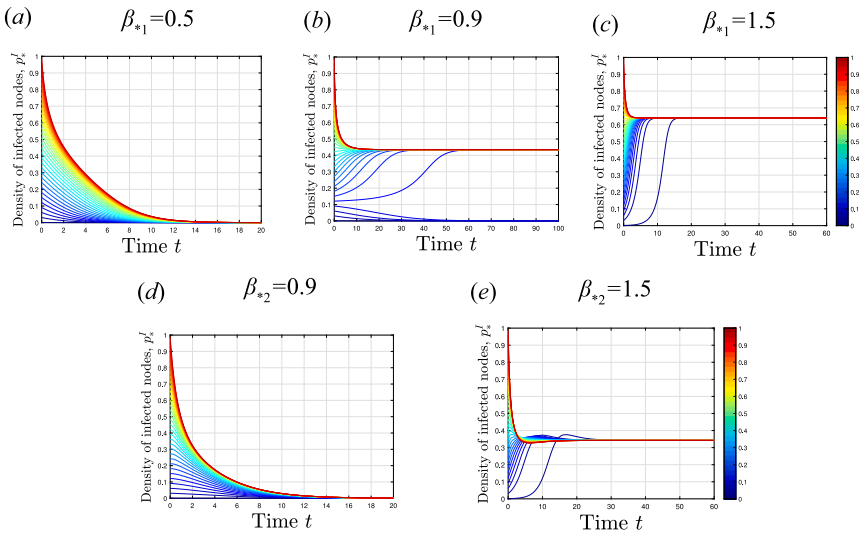

Fig. 6. The numerical solutions for the system under different initial values, where the information influence value $\gamma = 1$, (a) $\beta_{*1} = 0.5$, (b) $\beta_{*1} = 0.9$, (c) $\beta_{*1} = 1.5$, and when the information influence value $\gamma = 0.2$, (d) $\beta_{*2} = 0.9$, (e) $\beta_{*2} = 1.5$. β_{*1} represents the infectivity when $\gamma = 1$, and β_{*2} represents the infectivity when $\gamma = 0.2$. The horizontal axis represents Time t. The vertical axis represents density of infected nodes p^I_*.

Fig. 5(b) provides the numerical solutions of system (4) at $t = 500$, obtained by setting initial values as $[p^A(0) = 0.2, p^I(0) = 0.01, 0.2]$, confirming the stability of equilibrium points in the system. The results indicate that when $\gamma = 1$, the information network does not influence the physical contact network, and bistability phenomena occur due to the presence of higher-order structures (i.e., the coexistence of disease-free equilibrium and endemic equilibrium). As γ decreases, the bistability interval gradually shrinks until it disappears. In this case, given $\beta_{*1} = 0.9$ (β_{*1} represents the infectivity when $\gamma = 1$), there exist two stable equilibrium points within the non-negative interval, denoted as β^0_{*1} and β^c_{*1}, where β_{*1} satisfies $\beta^0_{*1} < \beta_{*1} < \beta^c_{*1}$, resulting in bistability as depicted in Fig. 6(b). Fig. 6(b) illustrates the numerical solutions of the system for different initial values. Depending on the initial values, the system tends towards either the disease-free or the endemic equilibrium point. Convergence to the disease-free equilibrium implies the eventual disappearance of the disease. Reaching the endemic equilibrium point indicates the outbreak and the density of infected nodes stabilizes at a certain value. When β_{*1} satisfies $\beta_{*1} < \beta^0_{*1}$ (as depicted in Fig. 6(a)), the system has a stable disease-free equilibrium point. However, when β_{*1} satisfies $\beta_{*1} > \beta^c_{*1}$ (as depicted in Fig. 6(c)), a stable endemic equilibrium exists in the system.

In conclusion, as shown in Fig. 5(b), the system reaches the stable endemic equilibrium because it is stable. When considering $\gamma = 0.2$, indicating a high influence from the information network on the physical contact network, there exists only one stable equilibrium within the non-negative interval, hence, the bistability phenomena disappear. When β_{*2}(β_{*2} represents the infectivity when $\gamma = 0.2$) satisfies $\beta_{*2} < \beta^c_{*1}$ (as depicted in Fig. 6(d)), the System (3) has a stable disease-free equilibrium, indicating convergence

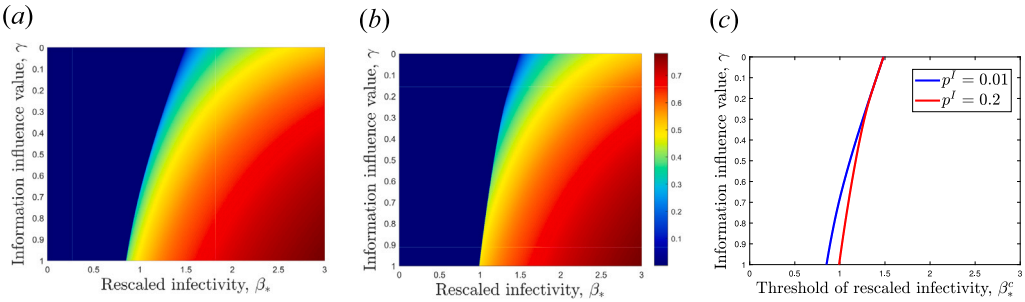

Fig. 7. The phase diagram of the coupled awareness-epidemic network, where (a) and (b) depict the steady-state heatmap obtained from the equations, (c) illustrates the change in threshold under different initial infection values as the information influence value γ decreases. The horizontal axis represents rescaled infectivity β_*. The vertical axis represents the information influence value γ.

to the stable disease-free equilibrium. When β_{*2} satisfies $\beta_{*2} > \beta_{*1}^c$ (as depicted in Fig. 6(e)), a stable endemic equilibrium exists in the System (3). Overall, as γ decreases, the reverse bifurcation turns into a forward bifurcation, leading to the gradual disappearance of bistability. It is also observed that as γ decreases, the outbreak threshold β_{*2}^c increases. When $\beta_{*2} > \beta_{*2}^c$ (i.e., post-outbreak) and β_{*2} is fixed, the value of the endemic equilibrium decreases.

3.3.2. The heatmaps of steady-state

Furthermore, we further analyzed the steady-state obtained by the system, as shown in Fig. 7. Fig. 7(a) and (b) respectively represent the infection density achieved at steady state under different infection strengths and information impact values with initial infection densities at 0.2 and 0.01. The horizontal axis represents the infection strength, and the vertical axis represents the information impact value, which decreases gradually from 1 to 0. Fig. 7(c) represents the infection threshold curves for disease outbreaks as the information influence value γ decreases from 1 to 0, considering initial infection densities of 0.01 and 0.2, respectively.

The phenomenon observed is supported by Fig. 7(a) and (b), indicating that as the influence of information decreases, the threshold for infection gradually increases. Furthermore, upon further comparison, it is noted that the decrease in threshold observed in Fig. 7(a) is greater than that in Fig. 7(b). This suggests that as the influence of information weakens, the infection threshold for disease spread also correspondingly rises, and this trend varies under different circumstances. Simultaneously, curves depicting the changes in threshold with decreasing information impact value γ under different initial infection densities are plotted. In Fig. 7(c), it can be observed that the bistability range gradually shrinks until it disappears. This indicates that as the influence of information network increases, it negatively impacts the disease transmission process, effectively slowing down or eliminating the bistability phenomenon in physical contact network. This is because as γ decreases, the stability of System (2) transitions from forward bifurcation to backward bifurcation. Thus, better control of disease spread can be achieved.

Therefore, it can be concluded that the impact of information can affect the existence and stability of disease-free equilibrium and endemic equilibrium, thus determining the occurrence of forward and backward bifurcations, which are crucial reasons for the existence or absence of bistability. Furthermore, the outbreak threshold and stable infection states also vary with the value of information impact.

4. Conclusion

In summary, the proposed coupled awareness-epidemic model considers higher-order interactions and incorporates the influence of information network on physical contact network to study collective interactions. It was discovered that information networks trigger richer dynamic phenomena in disease spreading. Extensive experiments were conducted to test the dynamics of higher-order simplicial complexes on both real-world and synthetic networks composed of simplicial complexes. As the influence of information increases, the transition shifts from discontinuous to continuous, leading to the gradual disappearance of bistability phenomena generated by higher-order structures, which indicates a trend towards greater stability in epidemic outbreaks. Theoretical analysis based on mean-field approximation was performed on the coupled awareness-epidemic model considering higher-order interactions. The results show that with increasing information influence, system stability transitions from forward bifurcation to backward bifurcation and the system's stability is enhanced.

Furthermore, introducing information networks into epidemic models plays a suppressive role in disease propagation. Theoretical and simulation results emphasize the significant role of information networks in disease propagation with higher-order structures. The stability of equilibrium is demonstrated to aid in understanding the system's stability. In practical scenarios, effective information dissemination can inhibit disease transmission, reduce the risk of disease outbreaks due to population aggregation, and raise the threshold for disease outbreaks and occurrences. Future research can be directed to investigate other complicated interaction patterns between information networks and physical contact network.

While this study provides important insights into the role of information networks and higher-order interactions, it adopts a simplified SIS model, neglecting factors of incubation, vaccination, quarantine. Future work could extend the model by incorporating

these factors to further enhance its relevance to real-world scenarios and provide more precise epidemic prevention strategies. Additionally, the model assumes idealized network structures and focuses on the dynamics of higher-order interactions without fully addressing the structural differences between the information and contact networks. The structure of the information network, typically modeled as a social network, differs significantly from the physical contact network in terms of properties such as degree distribution, clustering, modularity, and heterogeneity. These structural features can profoundly affect the diffusion of information and, consequently, the spread of disease. Future research could explore how different network structures impact the interplay between information dissemination and disease transmission, providing deeper insights into these complex dynamics.

CRediT authorship contribution statement

Xiangyu Meng: Writing – review & editing, Writing – original draft, Visualization, Investigation, Data curation, Conceptualization. **Wei Wei:** Writing – review & editing, Writing – original draft, Supervision, Resources, Methodology, Funding acquisition. **Xiangnan Feng:** Writing – review & editing, Writing – original draft, Supervision, Resources, Methodology, Formal analysis. **Zhenyu Shi:** Writing – review & editing, Writing – original draft, Software, Methodology, Formal analysis. **Baifeng Li:** Visualization, Validation, Software, Project administration, Formal analysis, Data curation.

Declaration of competing interest

The authors declare that they have no known competing financial interests or personal relationships that could have appeared to influence the work reported in this paper.

Acknowledgments

This work is supported by the National Natural Science Foundation of China (Grant Nos. 62276013, 62141605, 62050132), the Beijing Natural Science Foundation, China (Grant No. 1192012), and the Fundamental Research Funds for the Central Universities, China.

Appendix A. Augmentation techniques

The augmentation techniques involves extracting the list of sizes of the maximal simplices, also known as facets, and the list of pure simplicial degrees of nodes for each dataset. These lists are then duplicated five times, and the extended lists is applied as input to the simplicial configuration model. This process generates simplicial complexes that maintain the statistical characteristics of the original complex but are substantially larger in size.

Appendix B. Microscopic Markov chain approach

We denote the probability of individual i being in states AS, AI, NS, and US at time step t by $p_i^{AS}(t)$, $p_i^{AI}(t)$, $p_i^{NS}(t)$, and $p_i^{US}(t)$, respectively. Additionally, at each time step, the normalization condition $p_i^{AS}(t)+p_i^{AI}(t)+p_i^{NS}(t)+p_i^{US}(t)=1$ must be satisfied. We propose using a probability tree to reveal the potential states of nodes and their transitions, as shown in Fig. 8. Based on Fig. 8, we derive the MMCA equations for coupled dynamics in multiplex networks using the total probabilities of different states. Let a_{ij} and b_{ij} represent the adjacency matrices supporting the UAU and SIS processes, respectively. C_{ijk} indicates whether three nodes i, j, and k are in the same positive disease 2-simplices (if they are, then $c_{ijk}=1$; otherwise, $c_{ijk}=0$). Assuming the absence of dynamic correlations, the transition probability of node i not being informed by any neighbors is $r_i(t)$, i not being infected by any neighbors when perceiving $q_i^A(t)$, and i not being infected by any neighbors when not perceiving $q_i^U(t)$.

$$\begin{aligned} r_i(t) &= \prod_j [1-a_{ji}p_j^A(t)\lambda], \\ q_i^A(t) &= \prod_j [1-b_{ji}p_j^I(t)\beta^A]\cdot\prod_{k,l}[1-\beta^\Delta\gamma c_{kli}p_k^I(t)p_l^I(t)], \\ q_i^U(t) &= \prod_j [1-b_{ji}p_j^I(t)\beta^U]\cdot\prod_{k,l}[1-\beta^\Delta c_{kli}p_k^I(t)p_l^I(t)]. \end{aligned} \tag{B.1}$$

Among them, $p_j^A=p_j^{AI}+p_j^{AS}$, $p_j^I=p_j^{AI}+p_j^{AS}$. Using Eq. (B.1), the microscopic Markov chain of the coupling process for each node i can be obtained.

$$\begin{aligned} p_i^{AI}(t+1) =& p_i^{AI}(t)(1-\mu_1)(1-\mu_2)+p_i^{US}(t)(1-r_i)(1-q_i^A) \\ &+ p_i^{AS}(1-\mu_2)(1-q_i^A)+p_i^{UI}(t)(1-r_i)(1-\mu_1), \\ p_i^{US}(t+1) =& p_i^{AI}(t)\mu_1\mu_2+p_i^{US}(t)r_iq_i^U+p_i^{AS}\mu_2q_i^U+p_i^{UI}(t)r_i\mu_1, \\ p_i^{AS}(t+1) =& p_i^{AI}(t)(1-\mu_2)\mu_2+p_i^{US}(t)(1-r_i)q_i^A+p_i^{AS}(1-\mu_2)q_i^A \\ &+ p_i^{UI}(t)(1-r_i)\mu_1, \\ p_i^{UI}(t+1) =& p_i^{AI}(t)(1-\mu_1)\mu_2+p_i^{US}(t)r_i(1-q_i^U)+p_i^{AS}\mu_2(1-q_i^U) \\ &+ p_i^{UI}(t)r_i(1-\mu_1). \end{aligned} \tag{B.2}$$

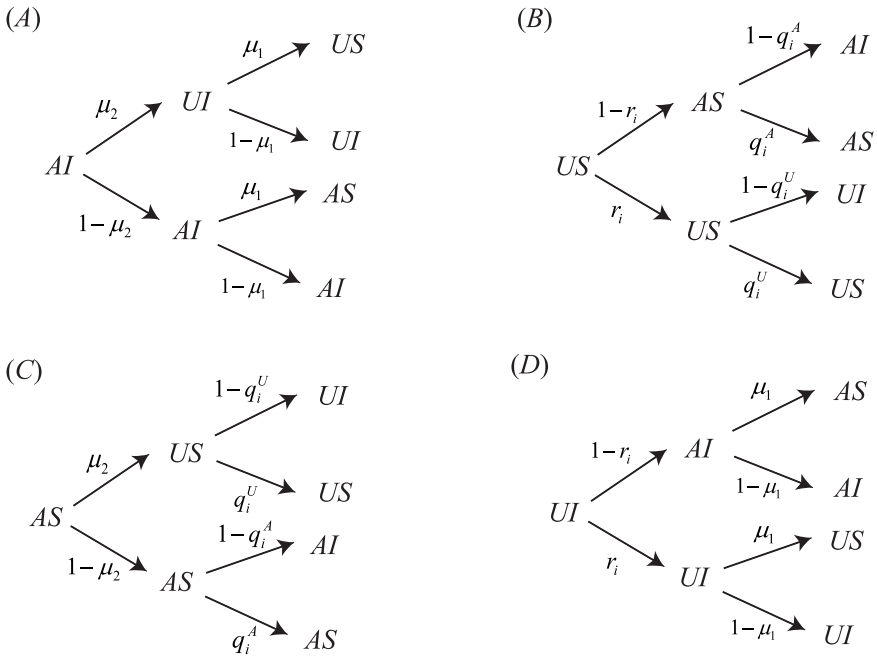

Fig. 8. UAU - SIS dynamic system state transition probability tree at each time step for states (A) AI, (B) US, (C) AS, and (D) UI. Denoted as (AI) Aware-Infected, (AS) Aware-Susceptible, (UI) Unaware-Infected, (US) Unaware-Susceptible, the transition probability from aware to unaware, the transition probability from infected to susceptible, the transition probability r_i from unaware to aware given by neighbors, the transition probability q_i^A from susceptible to infected given by neighbors if the node is aware, and the transition probability q_i^U from susceptible to infected given by neighbors if the node is unaware.

Data availability

Data will be made available on request.

References

[1] R. Albert, A.-L. Barabási, Statistical mechanics of complex networks, Rev. Modern Phys. 74 (1) (2002) 47.
[2] F. Radicchi, A. Arenas, Abrupt transition in the structural formation of interconnected networks, Nat. Phys. 9 (11) (2013) 717–720.
[3] A. Barrat, M. Barthelemy, A. Vespignani, Dynamical Processes on Complex Networks, Cambridge University Press, 2008.
[4] R. Pastor-Satorras, C. Castellano, P. Van Mieghem, A. Vespignani, Epidemic processes in complex networks, Rev. Modern Phys. 87 (3) (2015) 925.
[5] I. Iacopini, S. Milojević, V. Latora, Network dynamics of innovation processes, Phys. Rev. Lett. 120 (4) (2018) 048301.
[6] D.J. Watts, P.S. Dodds, Influentials, networks, and public opinion formation, J,. Consum. Res. 34 (4) (2007) 441–458.
[7] F. Wu, S. Zhao, B. Yu, Y.M. Chen, Y.Z. Zhang, A new coronavirus associated with human respiratory disease in China, Nature 579 (7798) (2020) 1–8.
[8] S.M. Poutanen, D.E. Low, B. Henry, S. Finkelstein, D. Rose, K. Green, R. Tellier, R. Draker, D. Adachi, M. Ayers, Identification of severe acute respiratory syndrome in Canada, N Engl J Med 348 (20) (2003) 1995–2005.
[9] S.W. Yoon, R.J. Webby, R.G. Webster, Evolution and ecology of influenza a viruses, Curr Top Microbiol Immunol (2014).
[10] H. Sun, Q. Guo, J. Qi, V. Ajjarapu, R. Bravo, J. Chow, Z. Li, R. Moghe, E. Nasr-Azadani, U. Tamrakar, Review of challenges and research opportunities for voltage control in smart grids, IEEE Trans. Power Syst. (2019) 1.
[11] P. Bora, Are internet videos useful sources of information during global public health emergencies ? A case study of YouTube videos during the 2015-16 zika virus pandemic, Pathog. Global Health 112 (6) (2018).
[12] H. Xu, Y. Zhao, D. Han, The impact of the global and local awareness diffusion on epidemic transmission considering the heterogeneity of individual influences, Nonlinear Dynam. 110 (1) (2022) 901–914.
[13] M. De Domenico, C. Granell, M.A. Porter, A. Arenas, Author correction: The physics of spreading processes in multilayer networks, Nat. Phys. 14 (5) (2018) 523.
[14] M. Lucas, I. Iacopini, T. Robiglio, A. Barrat, G. Petri, Simplicially driven simple contagion, Phys. Rev. Res. 5 (1) (2023) 013201.
[15] H. Leng, Y. Zhao, J. Luo, Y. Ye, Simplicial epidemic model with birth and death, Chaos 32 (9) (2022).
[16] Y. Pan, Z. Yan, The impact of multiple information on coupled awareness-epidemic dynamics in multiplex networks, Phys. A 491 (2018) 45–54.
[17] K.A. Kabir, J. Tanimoto, Analysis of epidemic outbreaks in two-layer networks with different structures for information spreading and disease diffusion, Commun. Nonlinear Sci. Numer. Simul. 72 (2019) 565–574.
[18] I. Iacopini, G. Petri, A. Barrat, V. Latora, Simplicial models of social contagion, Nat. Commun. 10 (1) (2019) 2485.
[19] C. Liu, Y. Yang, B. Chen, T. Cui, F. Shang, J. Fan, R. Li, Revealing spatio-temporal interaction patterns behind complex cities, Chaos 32 (081105) (2022).
[20] R. Li, W. Wang, Z. Di, Effects of human dynamics on epidemic spreading in cote d'ivoire, Phys. A 467 (2017) 30–40.
[21] J.L. Burton, Health and safety at necropsy, J. Clin. Pathol. 56 (4) (2003) 254–260.
[22] J.W. Tang, P. Wilson, N. Shetty, C.J. Noakes, Aerosol-transmitted infections—a new consideration for public health and infection control teams, Curr. Treat. Options Infect. Dis. 7 (2015) 176–201.
[23] R. Li, P. Richmond, B.M. Roehner, Effect of population density on epidemics, Phys. A 510 (2018) 713–724.

[24] C. Connell, McCluskey, Complete global stability for an SIR epidemic model with delay — distributed or discrete - ScienceDirect, Nonlinear Anal. Real World Appl. 11 (1) (2010) 55–59.
[25] Funk, Sebastian, Gilad, Erez, Watkins, Chris, Jansen, A.A. Vincent, The spread of awareness and its impact on epidemic outbreaks, Proc. Natl. Acad. Sci. USA (2009).
[26] C. Granell, S. Gómez, A. Arenas, Dynamical interplay between awareness and epidemic spreading in multiplex networks, Phys. Rev. Lett. 111 (12) (2013) 128701.
[27] C. Granell, S. Gómez, A. Arenas, Competing spreading processes on multiplex networks: awareness and epidemics, Phys. Rev. E 90 (1–1) (2014) 012808.
[28] Q. Guo, X. Jiang, Y. Lei, M. Li, Z. Zheng, Two-stage effects of awareness cascade on epidemic spreading in multiplex networks, Phys. Rev. E 91 (1–1) (2015) 012822.
[29] M. Sun, Y. Tao, X. Fu, Asymmetrical dynamics of epidemic propagation and awareness diffusion in multiplex networks, Chaos 31 (9) (2021).
[30] M. Sun, X. Fu, Competitive dual-strain SIS epidemiological models with awareness programs in heterogeneous networks: two modeling approaches, J. Math. Biol. 81 (1) (2023).
[31] D. Wang, Y. Zhao, J. Luo, H. Leng, Simplicial SIRS epidemic models with nonlinear incidence rates, Chaos 31 (5) (2021).
[32] R. Pastor-Satorras, C. Castellano, P.V. Mieghem, A. Vespignani, Epidemic processes in complex networks, Rev. Modern Phys. (2015).
[33] Hethcote, W. Herbert, The mathematics of infectious diseases, SIAM Rev. (2000).
[34] L.V. Gambuzza, F.D. Patti, L. Gallo, S. Lepri, S. Boccaletti, Stability of synchronization in simplicial complexes, Nature Commun. 12 (1) (2021).
[35] O.T. Courtney, G. Bianconi, Generalized network structures: The configuration model and the canonical ensemble of simplicial complexes, Phys. Rev. E 93 (6) (2016) 062311.
[36] SocioPatterns Collaboration, 2024, http://www.sociopatterns.org/ (Accessed July 2024).
[37] M. Génois, A. Barrat, Can co-location be used as a proxy for face-to-face contacts? EPJ Data Sci. 7 (1) (2018) 1–18.
[38] L. Isella, J. Stehlé, A. Barrat, C. Cattuto, J.-F. Pinton, W. Van den Broeck, What's in a crowd? Analysis of face-to-face behavioral networks, J. Theoret. Biol. 271 (1) (2011) 166–180.
[39] P. Vanhems, A. Barrat, C. Cattuto, J.-F. Pinton, N. Khanafer, C. Régis, B.-a. Kim, B. Comte, N. Voirin, Estimating potential infection transmission routes in hospital wards using wearable proximity sensors, PLoS One 8 (9) (2013) e73970.
[40] R. Mastrandrea, J. Fournet, A. Barrat, Contact patterns in a high school: a comparison between data collected using wearable sensors, contact diaries and friendship surveys, PLoS One 10 (9) (2015) e0136497.
[41] Jean-Gabriel, Young, Giovanni, Petri, Francesco, Vaccarino, Alice, Patania, Construction of and efficient sampling from the simplicial configuration model, Phys. Rev. E 96 (3) (2017).
[42] J.G. Young, G. Petri, F. Vaccarino, A. Patania, Construction of and efficient sampling from the simplicial configuration model, Phys. Rev. E 96 (3–1) (2017) 032312.
[43] Gomez, Aborge Holthoefer, Jmeloni, Y. Smoreno, Discrete-time Markov chain approach to contact-based disease spreading in complex networks, Europhys. Lett. 89 (3) (2010).
[44] I.D. Mayergoyz, Mathematical Models of Hysteresis, Mathematical Models of Hysteresis, 1991.
[45] Y. Wang, D. Chakrabarti, C. Wang, C. Faloutsos, Epidemic spreading in real networks: An eigenvalue viewpoint, in: International Symposium on Reliable Distributed Systems, 2003.